J Solid State Electrochem (2008) 12:409–420
DOI 10.1007/s10008-007-0431-0

ORIGINAL PAPER

Kinetics of electrochemically induced phase transitions in ion-insertion electrodes and the chemical diffusion coefficient

M. D. Levi · D. Aurbach

Received: 13 January 2007 / Revised: 23 August 2007 / Accepted: 5 September 2007 / Published online: 17 October 2007

Abstract In this paper, we report on the study, by numerical simulations, of the effect of slow external kinetics steps on the dynamics of electrochemically induced phase transitions in ion-insertion electrode materials. Two alternative kinetics steps such as slow interfacial ion transfer and slow small droplet formation were chosen to evaluate the errors in the calculation of the chemical diffusion coefficient, D, induced by incorrect application of non-equilibrium differential intercalation capacitances, C_{dif}. Comparison between simulated and experimental curves shows that for a moderate limitation of phase transition by Butler–Volmer kinetics, the exact values D can be obtained up to the composition of the binodal point, and then errors increase towards the spinodal domain. Within the spinodal domain, the potential dependence of D obtained formally by application of the Cottrellian model, entirely relates to the potential dependence of C_{dif}. The relevant description of phase transition dynamics in this region should include consideration of moving boundary between the coexisting phases formed via coalescing of growing nuclei.

Keywords PITT · GITT · EIS · Li-ion batteries · Intercalation · Nucleation and growth · Diffusion · Differential intercalation capacitance · Chemical diffusion coefficient

Introduction

Studying the electrochemical formation of some intermetallic alloys, such as Li_XAl and $Li_{1+Y}Sb$, Wen et al. [1] and Weppner and Huggins [2] elaborated on a simple and reliable method of determination of chemical diffusion coefficients (D) later called potentiostatic and galvanostatic intermittent titration techniques (PITT and GITT, respectively). Their approach was based on purely Fickian dynamics of the insertion process; hence, the contributions due to Ohmic potential drops or slow interfacial ion-transfer kinetics were disregarded in this work compared to the rate of solid-state diffusion of ions in the electrode bulk. The latter thus was considered as the single rate-determining step (RDS) of the insertion process. In principle, this approach can be easily adjusted to studying the insertion processes with strong concentration (or potential) dependences of D: In this case, the entire insertion process is divided in a sufficiently large number of small incremental potential (or current) pulses within which D remains to be constant [3]. One essential assumption about the correct application of PITT is that before applying the potential increment, the electrode is in equilibrium state with the concentration of ions, say, c_i, whereas at the end of the applied potential increment, the intercalation electrode reaches a new equilibrium state with the bulk concentration c_{i+1}.

As the above incremental techniques to which one can also add electrochemical impedance spectroscopy (EIS) treat the same situation of finite-space diffusion of ions in the electrode bulk [4], solutions to the diffusion equation with the different boundary conditions specific of the technique used allow to express the diffusion coefficient through the ratio of the characteristic diffusion kinetic parameters and the differential intercalation capacitance, C_{dif} [5]. For PITT, for example, D appears to be proportional to a squared ratio of the Cottrellian parameter, $It^{0.5}$, and the differential capacitance C_{dif} [5] From this simple consideration, it follows immediately that there can be two major sources of errors when determining D by PITT: (1) an incorrect evaluation of the diffusion parameter, $It^{0.5}$, as, e.g., Ohmic potential drops

Dedicated to Prof. O.A. Petrii's 70th birthday.

M. D. Levi (✉) · D. Aubach
Department of Chemistry, Bar-Ilan University,
Ramat-Gan 52900, Israel
e-mail: levimi@mail.biu.ac.il

and finite rates of interfacial ion-transfer are disregarded, and (2) an incorrect determination of C_{dif} for the systems undergoing phase transitions during ions intercalation (see later).

Recently, much attention was attracted to the former source of errors related to the fact that Ohmic and interfacial ion-transfer resistances may be comparable or even higher than the related diffusion resistance and that their ratio may be strongly potential-dependent resulting in the so-called "spurious" potential dependence of D [6–8]. Exact solution of diffusion equation with boundary condition related to slow interfacial charge transfer has been derived, which allows to produce (via non-linear fitting) the correct values of the kinetic parameter $It^{0.5}$ [9]. A much simpler method for correcting $It^{0.5}$ for the external kinetic contributions was recently proposed in which the explicit numerical solution to diffusion equation is replaced by certain simple approximations to this solution [10]. Practical application of this method has been reported in detail [11, 12].

In contrast, much less attention was paid in the literature to errors in D due to incorrect determination of C_{dif} for the intercalation systems undergoing phase transitions. In fact, first-order phase transition in an intercalation electrode under PITT conditions occurs by applying a single small potential step, so that the entire intercalation process cannot be presented by a sequence of titrations steps linking true equilibrium states with different concentrations of ions in the electrode bulk. Analysis of numerous literature data on electrochemically induced phase transitions in ion-insertion electrodes performed by PITT, GITT, and EIS forces us to adopt that different authors arbitrarily divide the two-phase domain into a number of titrations steps thus resulting in errors in C_{dif}, and due to this, in D. It is obvious that in this case, C_{dif} becomes strongly dependent on both the number of titrations and the nature of RDS of the phase transition. Note the important difference in the electrochemical behavior of ion-insertion electrodes in which intercalation proceeds in the form of a solid-solution and as a phase transition: In the former case, RDS other than diffusion directly affects the diffusion parameter ($It^{0.5}$) rather than C_{dif}, whereas in the case of phase transition, both $It^{0.5}$ and C_{dif} become dependent on these RDS.

The goal of this work is to perform numerical simulation of C_{dif} and D responses for an intercalation system with first-order phase transition complicated by one of the following slow kinetic steps: either slow interfacial charge transfer (Butler–Volmer kinetics) [13] or slow formation of droplets of a new phase in the bulk of the old one [14]. First-order phase transition in our numerical experiments was simulated in the framework of lattice-gas model with highly attractive interactions between the insertion sites [14, 15] (i.e., by Frumkin-type intercalation isotherms [5]). Starting from a set of values of C_{dif} and D calculated for the different intercalation levels of X within the mean-field theory for a system with a single diffusion RDS, we recalculate the same quantities taking into account the above alternative RDS of phase transition (Butler–Volmer kinetics and slow droplet formation). This is the proper way to analyze the errors in determination of D due to involvement in the intercalation process RDS other than diffusion, resulting in kinetically limited C_{dif}. It will be shown that in the case of slow Butler–Volmer kinetics, D appears to be unperturbed at the beginning of intercalation and, essentially, in the binodal domain; Two-phase domain (and hence the spinodal behavior) shifts in the course of intercalation (deintercalation) to lower (higher) potentials (with respect to equilibrium case) resulting in a deep minimum in D (reflecting maximum in C_{dif}) and signifying highly attractive interactions between the intercalation sites. In contrast, slow droplet formation decreases the maximum on the free energy curve (separating the diluted and concentrated phases) so effectively that the spinodal domain formally degenerates; the potential dependence of D and their absolute values has nothing in common with the values of D without external kinetic limitation. Comparison with experimental data for LiC_{12} to LiC_6 phase transition shows reliability of the scenario of phase transition involving slow Butler–Volmer kinetics.

"Differential capacitance and limiting kinetics of phase transition caused by ion insertion" of the Results and Discussion chapter introduces mean-field expressions for C_{dif} with and without two alternative kinetic limitations of phase transition mentioned above. In "Limiting kinetics of phase transition and the chemical diffusion coefficient," we concentrate on the mean-field expression of D with and without external kinetic limitations. Basic equation for the determination of D by PITT is compared here with the related mean-field expression, whereas the experimentally determined potential dependence of D with that followed from numerical simulations. Finally, "Comparison of the results of the above calculations work with predictions of phase field models" provides a more general view of what happens in the binodal and spinodal domains of phase transition by finding a correct place to nucleation and growth phenomenon in the time scale of the transition, introducing a concept of moving boundary and reconsidering our previous view of the origin of pseudo-Cottrellian behavior of lithiated carbon in the spinodal domain [16]. In general, our results are in agreement with basic predictions of phase-field models [17].

Results and discussion

Differential capacitance and limiting kinetics of phase transition caused by ion insertion

To follow the effect of limiting kinetics of phase transition on both C_{dif} and D, we will consider a mixed electron-ionic

conductor with the enhancement (thermodynamic) factor (W_i) of the form [18, 19]:

$$W_i = t_e\left[1 + \frac{z_i^2 c_i}{z_e^2 c_e}\right] \quad (1)$$

In this equation, z_i and c_i, and z_e and c_e are the charge and bulk concentration of ionic and electronic species, respectively; t_e is the electron transference number.

According to Eq. 1, W_i depends on both t_e and the ratio of the quantity z^2c for both conducting species. The value of W_i defines the shape of the intercalation isotherm and the distribution of potential across the current collector|insertion electrode|solution interfaces [18]. We further consider a particular and simplest case of an insertion compound with $c_e >> c_i$ and $t_e=1$ (metallic conductivity) resulting, according to Eq. 1, in the value $W_i=1$. The cases with W_i higher than 1, although complicate the related equations, are expected to be in qualitative agreement with the analysis for $W_i=1$.

For the enhancement factor equal to 1, the intercalation process can be conveniently presented by a simple Frumkin isotherm of the form [5, 14]:

$$f(E - E_o) = \ln\left(\frac{X}{1-X}\right) + g(X - 0.5) \quad (2)$$

In this equation, f is a combination of the Boltzmann constant, k, absolute temperature, T, and the electronic charge, e, $f = e/kT$. E and E_o are the electrode potential and its standard value, respectively, and X stands for the occupation number (intercalation level).

The shape of the intercalation isotherm (X vs E) or the related charging–discharging curve (E vs X) depends strongly on the effective dimensionless interaction parameter g. In case of the absence of ion–ion interactions, $g=0$. Under this circumstance, the Frumkin insertion isotherm reduces to a Langmurian-type isotherm [5, 14, 15]. The cases $g>0$ and $g<0$ are characteristic of the repulsive and the attractive interactions, respectively. When $g=-4$, the highly attractive interactions between the intercalation sites force the reaction to proceed as an ideal first-order phase transition at the standard potential.

Following the analysis of electrochemically induced phase transitions developed in [14], it is of interest to look at the mean-field expression for free energy of intercalation normalized per unit site, F_t/kTc_i (c_i=maximal concentration of the inserted ions). This can be easily obtained by integration of intercalation isotherm (Eq. 2) with respect to X:

$$\frac{\Delta F}{kTc_i} = -fX\,\Delta(E - E_o) + X\ln X + (1-X)\ln(1-X) - 0.5gX(1-X) \quad (3)$$

To demonstrate the essential electrochemical features of phase transition, we chose the case of highly attractive interactions between the intercalation sites with $g=-6$. Figure 1 presents the free energy as a function of X for the values of $(E-E_o)$ varying from −0.02 to 0.02 V. We will first consider deintercalation reaction (charging) when the electrode potential is swept towards more positive values. It is seen from

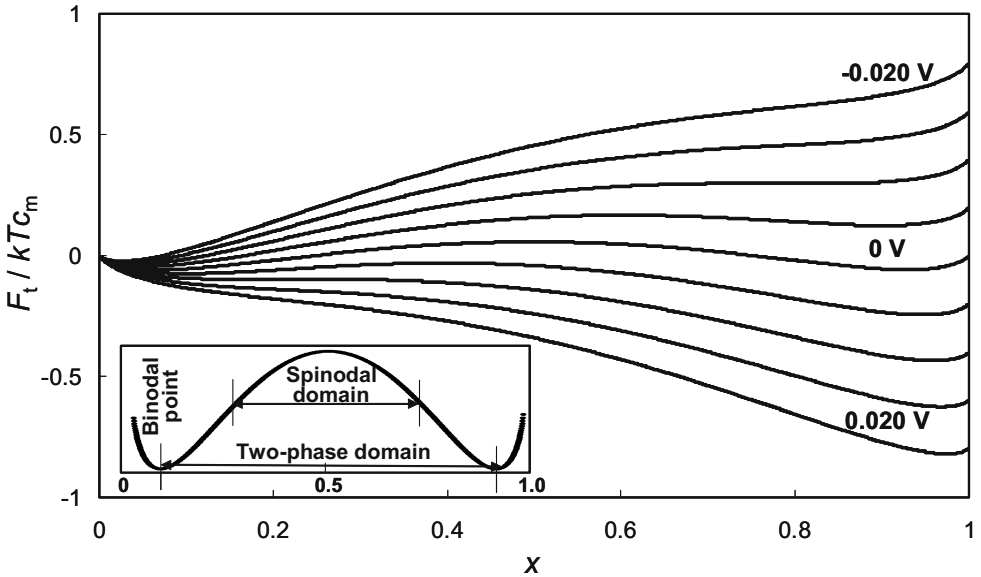

Fig. 1 The plot of the non-equilibrium free energy per unit site, F_t/kTc_m, vs the intercalation level, X, calculated from a mean-field expression (Eq. 3) for g=-6 (i.e., for highly attractive interactions between the intercalation sites which lead to a phase transition) for the range of potentials, $(E-E_o)$, varying from −0.02 to 0.02 V, with 5 mV steps. The *inset* in the figure is an enlarged view of the plot at the standard potential $E=E_o$ showing clearly the existence of an energy barrier between two minima (binodal points) corresponding to a two-phase domain. The points, in which the first derivative of F_t/kTc_m with respect to X (i.e., the chemical potential) passes through maximum and minimum, respectively, define the domain of the spinodal instability (see details in the text)

the curves in Fig. 1 that at $E-E_o<0$, a rather high maximum (hump) appears, which separates two minima with low and high ionic concentration, respectively. This barrier remains even at $E-E_o=0$ and starts to degrade with the further anodic polarization in a very narrow potential range: At $E-E_o=$ 10 mV, the hump completely disappears, thus initiating deintercalation reaction. Intercalation reaction (as $E-E_o$ shifts in the negative direction) can be regarded as the inverse process to deintercalation reaction, as is easily seen from Fig. 1: At $E-E_o=10$ mV, the curve has a high hump, which remains also at $E-E_o=0$; complete elimination of this peak occurs at $E-E_o=-10$ mV.

The inset in Fig. 1 shows an enlarged view of the free energy curve at the standard potential. The minima in this curve mark the so-called binodal points, whereas the points in which the first derivative of the curve passes through maximum and minimum (i.e., the inflection points on the free energy curve) mark the domain of spinodal instability [17]. The region between the binodal and the spinodal points is only metastable, and the related charging and discharging of the electrode may proceed in a single phase although the system free energy is not at its absolute minimum (as in the case of a solid solution quenched to this region [20]). Phase separation in the metastable region requires nucleation, which is ignored at this preliminary step of the analysis of the free energy curves.

We should specially emphasize that because of the existence of a rather high maximum in the free energy curve, which cannot be overcome in any equilibrium manner, the curve should be considered as essentially non-equilibrium: The beginning of intercalation and deintercalation reactions are separated by an intrinsic potential difference, the latter does not depend on the rate of the insertion and deinsertion processes and takes place at virtually zero charging rate with no involvement of any external kinetic processes. These external processes may seriously modify the shape of the isotherm and charging–discharging curves, which is presented later in this section.

The dimensionless differential capacitance without an interference of the external kinetics can be easily obtained by differentiation of the intercalation isotherm [5]:

$$\frac{C_{dif}}{fQ_m}=\left(g+\frac{1}{x}+\frac{1}{1-x}\right)^{-1} \tag{4}$$

In this equation, Q_m is the maximum available intercalation charge.

It is now appropriate to describe how the external kinetics modify the expression for C_{dif} under quasi-equilibrium or non-equilibrium conditions. Consider first a slow ionic transfer across the electrode-solution interface relevant to the condition $W_i=1$. In this case, C_{dif} can be conveniently defined in terms of cyclic voltammetry under the limitation of the insertion process by a Butler–Volmer kinetics. Cyclic voltammetry is used here as a convenient tool to vary the rate of the charging–discharging process through a single parameter, namely the scan rate, ν. However, qualitatively similar results are obtained when C_{dif} is evaluated by PITT in the case when the polarization time is not enough to reach a true thermodynamic equilibrium in each titration step (for first-order phase transition, the polarization time of separate titration steps may be intentionally decreased to have several titration points for the entire phase transition). In the considered case of $W_i=1$, the intercalation isotherm (Eq. 2) should be combined with the Butler–Volmer kinetic equation, meaning that no charging (discharging) occurs in the system until a certain potential is reached, which is sufficiently high to decrease the height of the maximum on the free energy curves, separating two different phases [5, 14]:

$$\begin{aligned}C_{dif}=(f\delta\nu/k_o)I_{dim}=(1-X)\exp[-(1-\alpha)gX]\\ \times\exp[(1-\alpha)f(E-E_o)]\\ -X\exp(\alpha gX)\exp[-\alpha f(E-E_o)]\end{aligned} \tag{5}$$

Here, I_{dim} is the dimensionless current; $K=(k_o/f\delta\nu)$ is the dimensionless rate constant, with k_o and ν representing the standard heterogeneous rate constant (cm s^{-1}) and the potential scan rate (Vs^{-1}), respectively, δ is the thickness of the host matrix (cm), and f was previously defined as F/RT. The charge-transfer coefficient, α, in Eq. 7 was assumed to be equal to 0.5, which is a reasonable initial approximation to many electrochemical reactions.

Numerical simulation of C_{dif} vs X curves for a chosen values of g, δ, α, and k_o was performed in the range of X from 0 to 1 with a step 0.001 using conventional Excel 2000 software. The entire domain of dimensionless intercalation level, X, was reverted to the domain of electrode potentials using numerical integration of the form:

$$(E-E_o)=Q_m\int_0^1 C_{dif}^{-1}dX \tag{6}$$

Using Eqs. 5 and 6, the differential capacitance curves were calculated for three representative scan rates (10, 40, and 200 μVs^{-1}) and, in addition, on the basis of Eqs. 4 and 6 for the process with no involvement of the external kinetics ($\nu=0$). These four curves for both insertion and deinsertion directions of the process are presented in Fig. 2a. The higher the scan rate, the larger is the overvoltage required to start the charging or the discharging process. Of great importance is the limit of very small scan rates approaching 0. The differential capacitance response according to Eqs. 5 and 6 is expressed by a δ-function, so that X runs all the values from

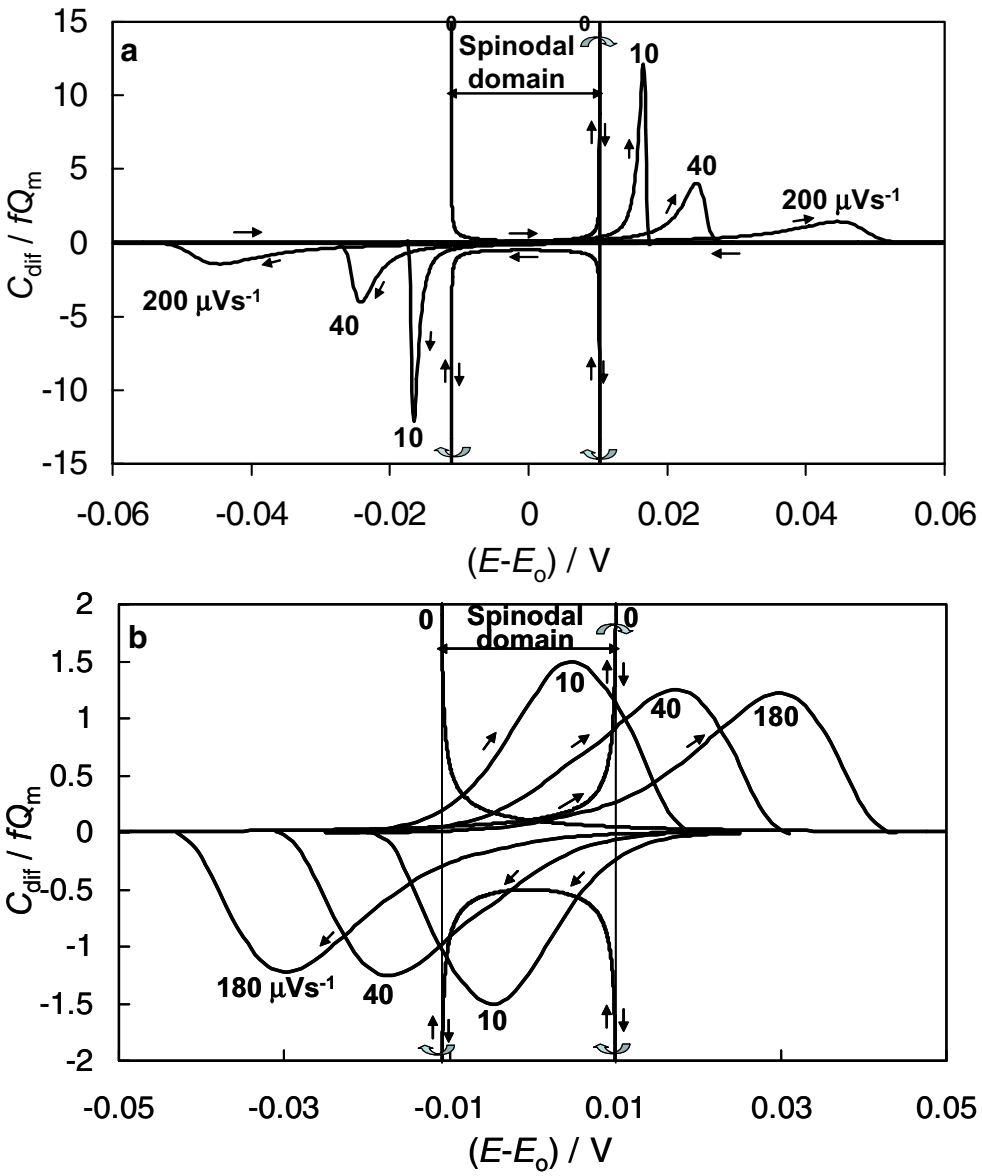

Fig. 2 Plots of quasi-equilibrium and non-equilibrium differential capacity of an intercalation electrode, C_{dif}/fQ_m, vs the electrode potential, $(E-E_o)$, calculated for a case of the kinetic control of a phase transition: **a** by slow interfacial charge transfer, and **b** by slow droplet formation (Eqs. 5 and 7, respectively). Different scan rates used (in μVs^{-1}) are indicated. The values of the parameters: $k_o=3.9\times10^{-4}$ cm s^{-1}, $\delta=10$ μm, $\omega=8.8\times10^{-3}$ s^{-1}, $n=8$, $g=-6$, and $f=38.9$ V^{-1}. The spinodal domain characterizing quasi-equilibrium charging–discharging (Eq. 4, scan rate formally approaches 0) is shown on both panels for the comparison

0 to 1 practically at the same potential (right hand point in the spinodal domain shown in Fig. 2a). This behavior is expected to appear in the experimental curves for phase transition processes when no external kinetics are involved. In contrast, application of Eqs. 4 and 6 for the calculation of C_{dif} allows for tracing directly the maximum in the free energy curve, as if an ideal relaxation process would permit tracing through its top (not a practical case). The related formal response of C_{dif} can be seen in Fig. 2a: At the right hand point of the spinodal domain, the differential capacitance approaches to $+\infty$, then reverts to $-\infty$ and remains negative down to the left hand point of the spinodal domain. Then the response reverts from $-\infty$ to $+\infty$ and decays to 0 at the right hand point of the spinodal domain.

Following Vorotyntsev and Badiali [14], we can assume a possible scenario of diminishing (degradation) of the maximum in the free energy curve alternative with respect to the previously considered case of dominance of the Butler–Volmer kinetics over entire phase transition. This implies formation of small droplets containing only several intercalation sites (n). Neglecting ripening of these droplets in time (disregard of a surface energy term in the expression for free energy, a conventional assumption in the zeroth approximation to phase separation in large systems [20]) results in the expression of C_{dif} in the following form [14]:

$$C_{dif}/fQ_m = (\omega/2\pi f\nu)(1-X)\exp(-nE_a/kT) \quad (7)$$

In this equation, ω is the characteristic frequency of droplets formation. The values of E_a for each potential $(E-E_o)$ are taken from the related heights of the peak in the free energy curve shown in Fig. 1. It is expected that a decrease in the value of n rises the exponent in Eq. 7, and hence, the

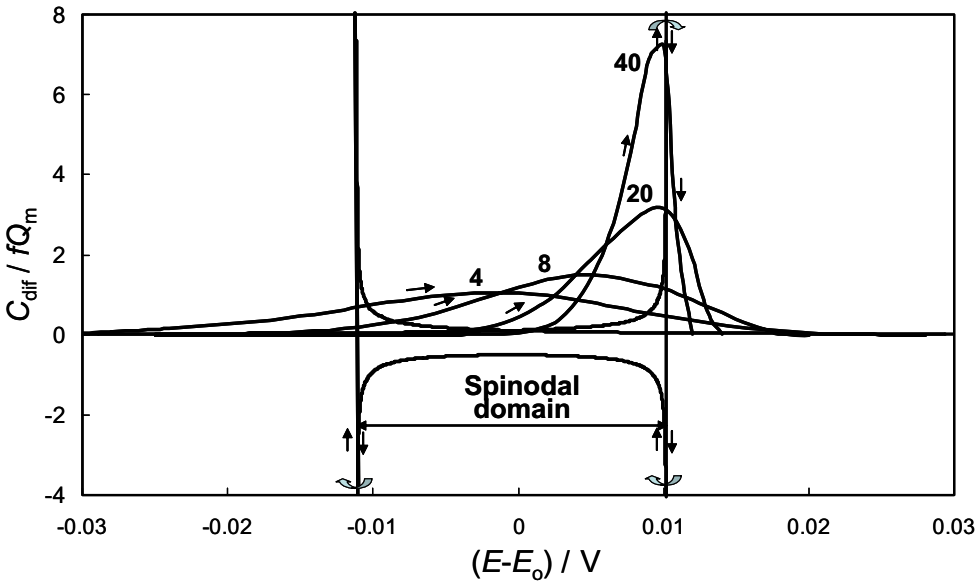

Fig. 3 The anodic branches of the plots of differential capacity *vs.* potential calculated for different numbers of sites, *n*, (the values are indicated near the curves) forming droplets of a new phase in the bulk of the old one

resulting droplet formation of a new phase will considerably decrease the overvoltage of the entire phase transition, shifting the beginning of charging (discharging) of the electrode to lower potentials.

Assuming arbitrarily in Eq. 7 that n=8 (see discussion of values of n below), the C_{dif} vs potential curves were simulated for different values of ν: 10, 40, and 180 μVs^{-1} (see Fig. 2b). Like for the previously considered case of Butler-Volmer limiting kinetics (Fig. 2a), the decrease in the scan rate enables the phase transition at lower overpotential. However, comparison between the curves in Fig. 2a and b also reveals important differences: (1) the half-peak widths in the latter case are much broader than for the former case, and most importantly, (2) the decrease in the scan rate for the droplet formation model pushes the intercalation reaction inside the degraded spinodal domain. In other words, formation of small droplets lowers the free energy barrier drastically, so that the spinodal region simply vanishes.

In Fig. 3, the calculated C_{dif} vs potential curves are shown for n equal to 4, 8, 20, and 40 (C_{dif} for ideal phase transition is shown for comparison). Evidently, the overvoltage considerably decreases as n becomes smaller. It is natural to expect that in the limiting case of a droplet including all the available intercalation sites (i.e., n approaching $+\infty$), no gain in the free energy occurs, and the situation returns to the ideal phase transition described above.

It is of interest to transform the results on C_{dif} obtained for both alternative kinetic limitations of phase transition to that in the form of voltage pictures: Galvanostatic technique is more frequently used for electrodes characterization than cyclic voltammetry. For this purpose, the curves in Fig. 2a and b are numerically integrated with respect to potential, and the results are shown in Fig. 4a and b, respectively. In full agreement with the above analysis of C_{dif} under the Butler–Volmer kinetic control, the decrease in ν flattens the potential plateaus and diminishes hysteresis of potentials between the charging and the discharging processes. Very small scan rate (an analog of a small current in the gal-

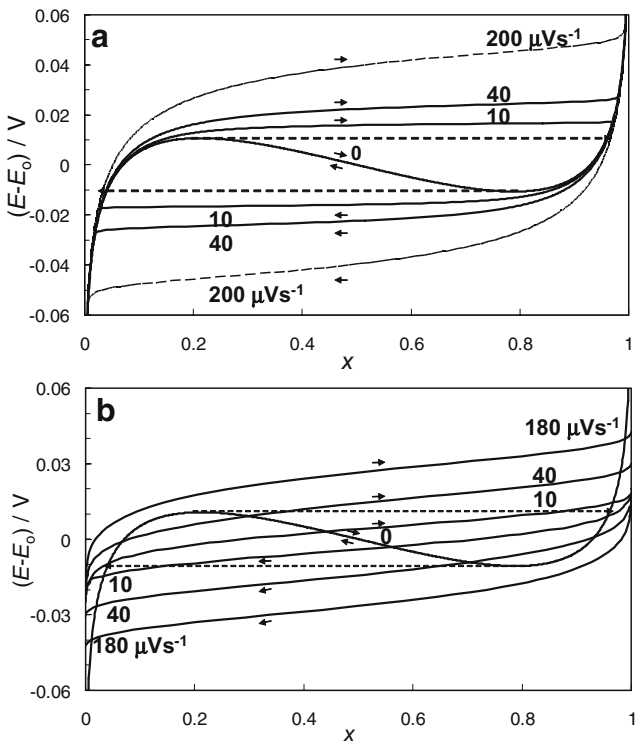

Fig. 4 Plots of quasi-equilibrium and non-equilibrium charging and discharging curves in the framework of two alternative models (**a** — for slow interfacial charge transfer, and **b** — for slow droplet formation) calculated by numerical integration of the differential capacity curves from panels a and b of the previous Fig. 2 using Eq. 6. The dotted lines mark the boundaries of the spinodal domain

vanostatic technique) makes the plateau completely horizontal; however, the potential hysteresis between charging and discharging still remains. In contrast, small droplets formation flattens the plateaus with decreasing ν only moderately. However, the hysteresis in the potentials between the electrodes's charging and discharging definitely reduces as ν decreases. This reflects degradation of the spinodal domain of phase transition (i.e., the domain of intercalation levels in which a maximum of the free energy exists) as previously discussed. However, because at higher scan rates potential hysteresis exists for both alternative limiting kinetics and it is not always experimentally clear which scan rate should be considered as small, we extend our analysis to consideration of the chemical diffusion coefficient, D, and its dependence on the rate of charging and discharging via the differential intercalation capacitance, C_{dif}. It is shown in the next section that potential dependences of D for the two alternative limiting kinetics of phase transition have qualitatively different features and hence may serve as a practical criterion to distinguish between them.

Limiting kinetics of phase transition and the chemical diffusion coefficient

The mean-field theory offers the following general expression for the chemical diffusion coefficient, D, as a function of the intercalation level [15]:

$$\frac{D}{D_{\mathrm{o}}} = X(1-X)\frac{(\partial \mu_{\mathrm{Li}^+}/kT)}{\partial X} \tag{8}$$

which takes a simple form in the case of a Frumkin-type isotherm [5]:

$$\frac{D}{D_{\mathrm{o}}} = \frac{X(1-X)}{C_{\mathrm{dif}}/fQ_{\mathrm{m}}} \tag{8a}$$

In this equation, $\mu_{\mathrm{Li+}}$ and D_{o} are the chemical potential of the inserted ions and the self-diffusion coefficient, respectively.

Equation 8a clearly shows that from a mean-field theory point of view, the normalized (scaled) chemical diffusion coefficient is defined as a ratio between the statistical factor of occupation of sites, $X(1-X)$ and the differential capacitance. The statistical factor is always expressed by a peak-shaped curve with maximum at X=0.5. Consideration of Eq. 8a along with Eq. 4 for C_{dif} shows that $D/D_{\mathrm{o}} = 1$ for g=0 and that the diffusion coefficient may pass through a deep minimum in the case of highly attractive interactions because the differential capacitance (C_{dif}) passes through a sharp maximum at the same values of X.

From an experimental point of view, D is expressed by the following formulae (PITT technique) [1, 2, 5]:

$$D = \pi l^2 \left[\frac{\left(It^{0.5}/\Delta E\right)}{C_{\mathrm{dif}}}\right]^2 \tag{9}$$

where l is the electrode thickness (or particle size [21]) and $It^{0.5}$ is the Cottrell diffusion parameter discussed above.

For a direct comparison between a mean-field expression, Eq. 8a, and the basic equation of PITT technique, Eq. 9, it is convenient to rewrite the latter equation in the equivalent form:

$$\frac{D}{D_{\mathrm{o}}} = \frac{\pi l^2}{D_{\mathrm{o}}(fQ_{\mathrm{m}})^2}\frac{\left(It^{0.5}/\Delta E\right)^2}{(C_{\mathrm{dif}}/fQ_{\mathrm{m}})}\frac{1}{(C_{\mathrm{dif}}/fQ_{\mathrm{m}})} \tag{9a}$$

From this comparison, it is clear that the product of the first two members in Eq. 9a should be simply equal to the statistical factor $X(1-X)$. Interestingly, the diffusion (Cottrell) parameter, $It^{0.5}$, depends on the attraction constant g in such a way that the change in its square compensates entirely the related change in the differential intercalation capacitance.

Equations 8a and 9a constitute a reliable basis for distinguishing between the limiting kinetics of phase transition by both a numerical simulation and experimentally. We consider first the results of the numerical simulations. C_{dif} values for the limiting Butler–Volmer kinetics and the slow droplet formation are given by Eqs. 5 and 7, respectively, so that simulation of D vs X plots (and taking into account Eq. 6, D vs E curves) using Eq. 8a becomes straightforward. Figure 5a and b present the potential dependences of D for the two limiting kinetics, respectively, using non-equilibrium (i.e. scan rate dependent) values of C_{dif}.

Assuming the Butler–Volmer kinetics to be the relevant RDS of phase transition, it is seen from Fig. 5a that a decrease in the scan rate makes the minimum of D vs E curve more sharp and, in addition, pushes it closer to the spinodal domain, a characteristic of phase transition, without external kinetic limitation. The latter ideal transition reveals a loop with negative values of D in the spinodal domain, which *cannot be observed in practice*, as one or another kinetic step controls the rate of phase transition. Estimations of the errors in D/D_{o}, which do not strictly relate to equilibrium values of C_{dif} obtained, e.g., at a scan rate of 10 μVs^{-1}, are better visualized in Fig. 6, where D/D_{o} is presented as a function of X. From the beginning of intercalation and up to the composition of the binodal point, the chemical diffusion coefficient calculated for small ν is 100% reliable at the slowest scan rate used (a few μVs^{-1}). For compositions related to the middle between the binodal and the spinodal points, the error is close to 20% and further drastically increases when approaching the point of spinodal instability. Formally small but positive values of the scaled diffusion coefficient, D/D_{o}, calculated for E or X inside the spinodal

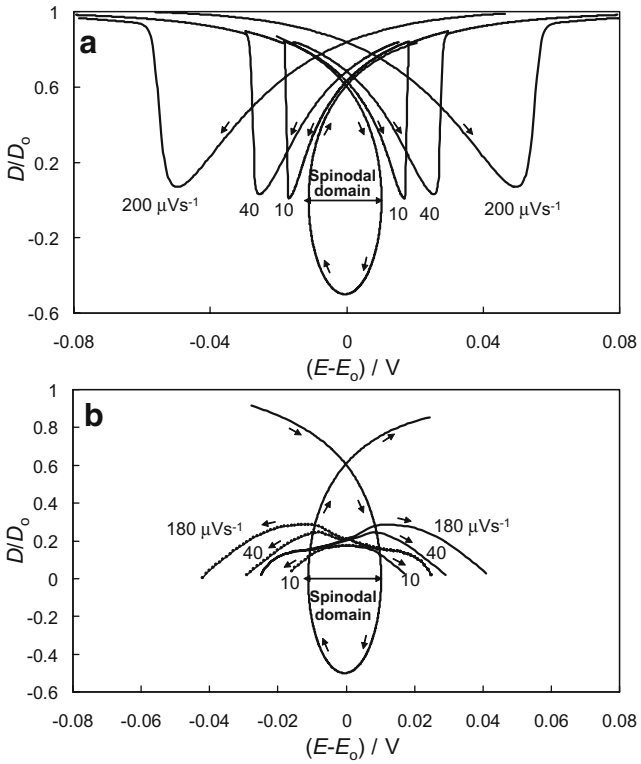

Fig. 5 Plots of the scaled (normalized) chemical diffusion coefficient, D/D_o, vs electrode potential, $(E-E_o)$, calculated for two alternative models of kinetic control of electrochemical phase transition reactions (Eq. 8a): **a** by a slow interfacial charge transfer limitation, and **b** by a slow droplet formation. C_{dif} for these calculations were obtained by simulated slow scan rate CV at different scan rates (in μVs^{-1}). The values of the parameters used were indicated in captions to Fig. 2. The spinodal domain with a characteristic loop of the formally negative values of the diffusion coefficient (combination of Eq. 4 and 8a with C_{dif} values calculated close to equilibrium situation, e.g., from cyclic voltammetry curves at a scan rate approaching 0) is shown in both panels for the comparison

domain indicate interfacial kinetic limitations of the phase transition. Note also that the error in D increases as the values of C_{dif} become far from their "equilibrium" values (i.e., evaluated at higher scan rates).

Drastically different potential dependence of D/D_o is observed when phase transition is limited by a slow droplet formation (see Fig. 5b). In this case, D/D_o remaining positive within the whole intercalation domain reveals a flat maximum, which somewhat increases when the differential capacity is calculated from cyclic voltammetry at higher scan rates. Thus, in contrast to the behavior of C_{dif} as a function of potential, which is somewhat similar in shape in both cases of kinetic limitations discussed here, the potential dependences of D/D_o can be easily used to distinguish between the alternative kinetic steps of phase transition.

To elucidate the reason of quite a different behavior of the potential dependences of D/D_o for the different kinetic limitations, we present the plots of D/D_o and its two constituents: the statistical factor, $X(1-X)$ and the differential intercalation capacitance, C_{dif}/fQ_m, as functions of X for the two alternative models in Fig. 7a and b. Note that the same plot of $X(1-X)$ appears in both panels of Fig. 7; hence, according to Eq. 8a, the difference in the shape of the D/D_o is entirely related to the difference in C_{dif} for both models. In fact, for the Butler–Volmer limitation of a phase transition, the peak of C_{dif} shifts to higher values of X compared to that for the ideally symmetric peak of $X(1-X)$. This predefines a deep, asymmetric minimum in D/D_o starting from the binodal point (X=0.07) and ending at X=0.97 as C_{dif}/fQ_m approaches zero. In contrast, for a limitation by small droplets formation (i.e., nucleation), C_{dif}/fQ_m vs X plot is much less asymmetric (compared to that of the former possibility) revealing a maximum at approximately X=0.5, i.e., at the same value of X in which the statistical factor $X(1-X)$ has a maximum. In addition, the slopes of both two curves are very similar in a wide range of X, which explains the flatness of the resulting D/D_o vs X plot. The absolute values of C_{dif}/fQ_m are about five times higher than that of $X(1-X)$; therefore D/D_o does not exceed 0.2 in the whole range of X.

Finally, Fig. 8a shows all the above three plots as functions of potential for the Butler–Volmer limitation of phase transition, whereas in Fig. 8b, we present the same plots

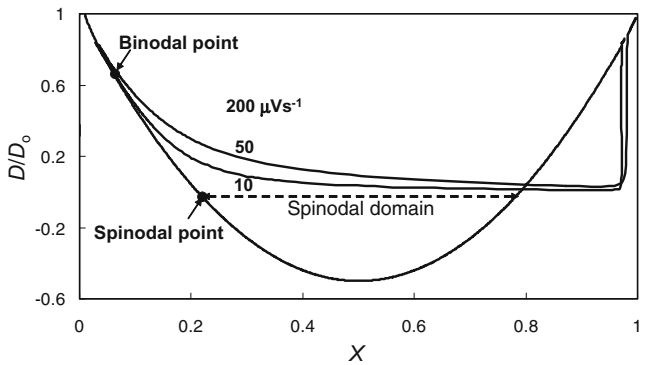

Fig. 6 Plots of the dimensionless chemical diffusion coefficient, D/D_o, vs intercalation level, X, calculated for the case of slow interfacial charge transfer. C_{dif} values, needed for the calculations, were obtained from simulated cyclic voltammetry curves at different scan rates. The relevant scan rates are indicated. The spinodal domain with formally negative values of D is shown for the comparison

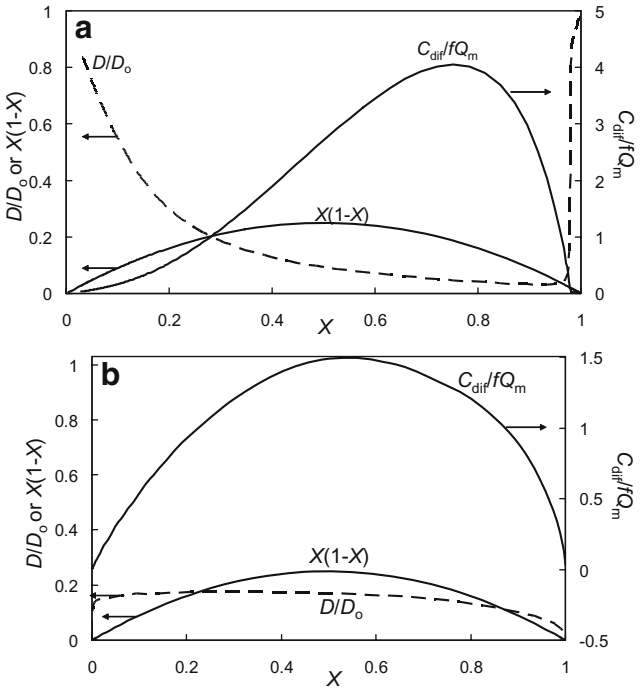

Fig. 7 Plots of the chemical diffusion coefficient, D/D_o, the contributing factors, $X(1-X)$ and C_{dif}/fQ_m vs intercalation level, X, (Eqs. 5, 7, and 8a) for two different models of kinetic control of phase transitions: **a** by slow interfacial charge transfer and **b** by slow droplet formation. The relevant scan rates are indicated

calculated from the experimental data for the electrochemically induced LiC_{12} to LiC_6 phase transition [12, 22]. Their qualitative similarity is spectacular. Hence, we can conclude that the above phase transition process is most probably influenced by a slow interfacial ion transfer kinetics.

Comparison of the results of the above calculations work with predictions of phase field models

Analysis of the chemical diffusion coefficient determined under a moderate limitation by the Butler–Volmer kinetics shows that it does not interfere a Fickian diffusion (provided that this diffusion model is appropriate) along the following domain of X: from the beginning of the intercalation process up to the middle between the binodal and spinodal points on the free energy curve as a function of the intercalation level or potential. Hence, the diffusion coefficients determined from the Cottrellian expression (Eq. 9), when using appropriately PITT or GITT techniques, remain reliable in this range of ion concentrations. Interestingly, similar conclusion for the same range of X was drawn in a recent paper devoted to application of a phase field model with relatively high gradient energy coefficients for the interpretation of the results of PITT and GITT measurements [17]. Their analysis was based on the assumption that C_{dif} is an equilibrium quantity, meaning the absence of any kinetic limitation. Hence, similarity in the results followed from both models means that C_{dif} values obtained at a practical rate of about 10 μVs^{-1} relate to essentially quasi-equilibrium situation (compare Figs. 2a, 4a, and 5a). Higher scan rates (or higher rates of charging–discharging) obviously result in higher deviations of the system from the classical Cottrellian behavior (due to errors in the precise calculation of C_{dif}, which leads to errors in the calculation of D vs X or E).

Phase-field models predict spontaneous phase separation once the concentration of ions enters into the spinodal domain without explicitly tracking the interface between the two coexisting phases [17, 20] (the approach based on direct tracking of the interface has been previously reported [16]). A Fickian model does not work in this concentration range at all, and the chemical diffusion coefficient formally takes negative values within the spinodal domain when treated in the framework of a lattice gas model. The phase field model predicts movement of the boundary between the coexisting phases [17]. Even moderate dominance of Butler–Volmer kinetics over the process of phase transition results in shifting the two-phase domain towards higher overvoltages, as at a certain overvoltage, only the maximum on the free energy curve degrades sufficiently to induce ions intercalation in the form of phase transition. The calculated chemical diffusion coefficient under the Butler–Volmer limitation of a phase transition exhibits a deep minimum (the values are of course

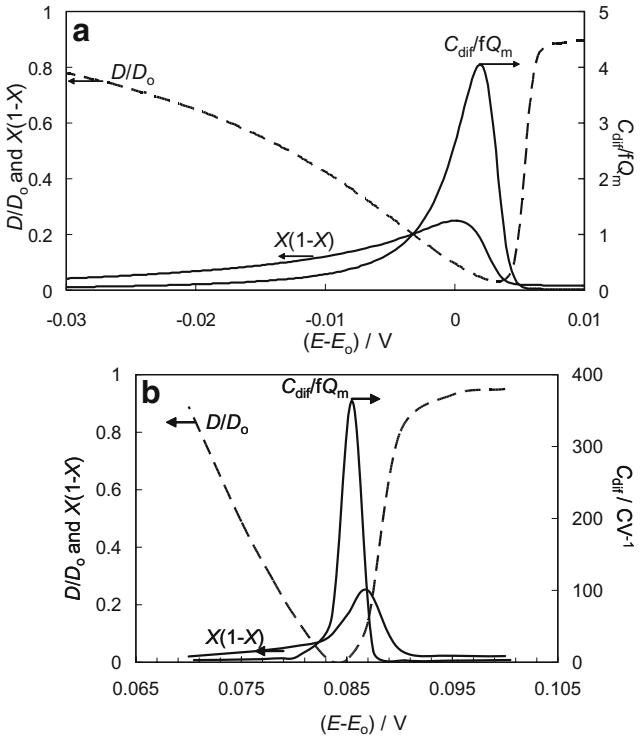

Fig. 8 Plots of the chemical diffusion coefficient, D/D_o, and the contributing factors, $X(1-X)$ and C_{dif}/fQ_m vs electrode potential, $(E-E_o)$ calculated for slow interfacial charge transfer (**a**) and the related experimental curves for LiC_{12} to LiC_6 phase transition (calculated from the data reported in Levi et al. [22]) (**b**)

always positive) originating from a maximum in C_{dif}, which becomes very narrow when obtained from cyclic voltammetry in the limit of slow rates of charging–discharging.

It is interesting that at relatively small rate of charging and discharging, the phase-field model predicts an almost constant velocity of the moving boundary during almost the entire period of phase transition [17]. This is not in line with previously reported data on electrochemical insertion of Li-ions into composite graphite electrodes [16] and highly ordered pyrolytic graphite (HOPG) [23]. From the related chronocoulometric data and simple moving boundary model, it was found that initially, the boundary changes its location (ξ) proportionally with time (i.e., the boundary propagates at a constant velocity), see Fig. 9a. However, at longer times, the boundary starts to move slower: the location of the boundary changes proportionally to square root of time [16], as shown by the lower curve in Fig. 9b. As the change in the location of the boundary according to this model is proportional to the charge injected during the insertion process, this allowed for the calculation of D within the alternative Cottrellian model (Eq. 9), see the pseudo-Cottrellian curve in Fig. 9b (the dotted line represents the pseudo-Cottrellian slope from which D was calculated). Diffusion coefficients obtained formally in the framework of both alternative models appeared to be very similar for the spinodal domain of the LiC_{12} to LiC_6 phase transition under consideration [12, 16, 22].

Analysis of numerical simulations performed in this work allows us to propose a reasonable explanation of the above similarity in D. Once a phase transition process is controlled by the Butler–Volmer kinetics, the minimum in D, roughly corresponding to the peak in C_{dif}, is somewhat shifted towards finite-space domain of the insertion process (see Fig. 8a). The charge-transfer resistance across the electrode-solution interface is constant during the applied potential step, and this may predetermine constant velocity of the moving boundary at short time. However, at longer times, the current decays in the finite-space domain of the intercalation process, producing a sharp maximum of the Cottrellian parameter, $It^{0.5}$, from which D is formally calculated. The pseudo-Cottrellian maximum actually originates from coupling of very slow interfacial kinetics with the finite-space decay of the current during intercalation as was previously suggested theoretically [9, 10] and verified experimentally [11, 12]. This maximum has clearly nothing in common with the Cottrellian diffusion, which cannot take place under the condition of phase separation. The above coupling of interfacial ion-transfer control with finite-space character of

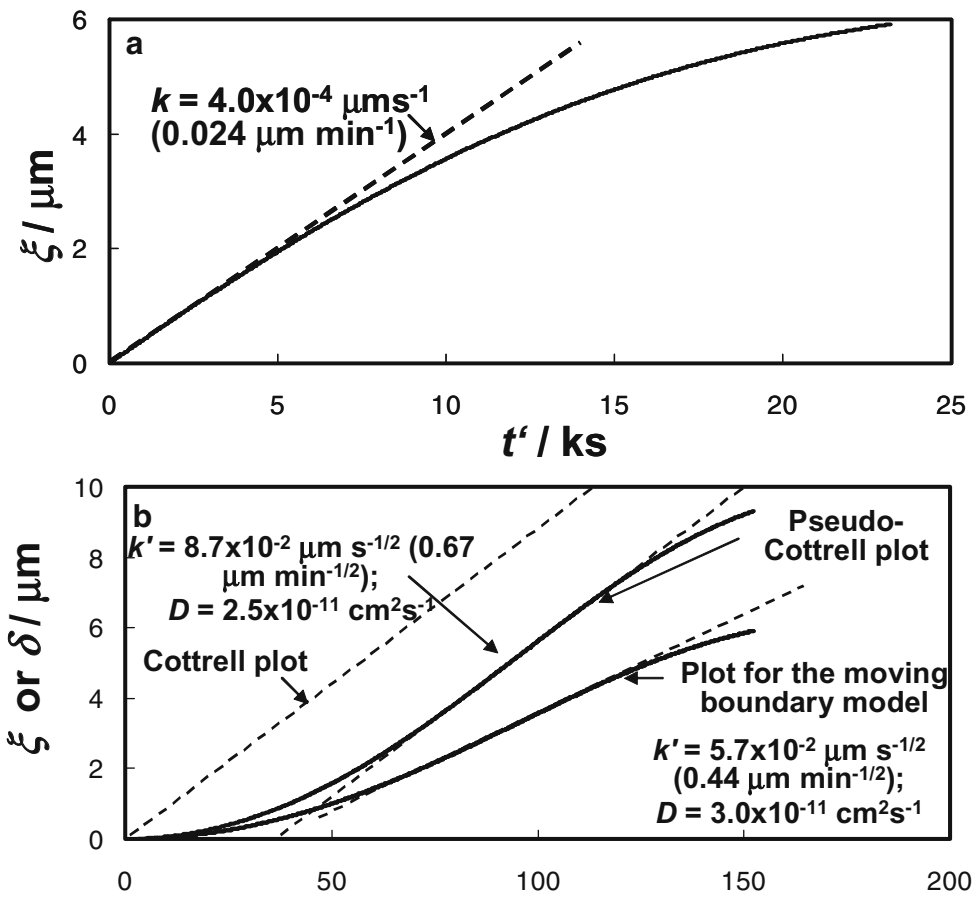

Fig. 9 Model treatment of the current vs time transient obtained at the beginning of a first-order phase transition, $LiC_{12} \rightarrow LiC_6$ in terms of a linear (**a**) and a square root (**b**) dependences of the moving boundary location, ξ ($0<\xi<l/2$; details in [16]). k and k' denote the related coefficients in the expressions $\xi=kt'$ and $\xi=k't'^{1/2}$ (see **a** and **b**, respectively.) The corrected time t' was obtained by subtracting the time of the nucleation process from the total time of the current transient. The pseudo-Cottrell plot was obtained using Eq. 9. The coefficient k', which was evaluated from the equation, $\delta=k't'^{1/2}$, and the related diffusion coefficient are indicated. The Cottrell plot denoted by *broken line* was constructed by shifting the linear portion of the quasi-Cottrellian plot along abscissas axis to the origin

the intercalation process may be the reason for changing the character of phase boundary movement from a linear to the square-root law.

Finally, we wish to comment on the small droplets limitation of a phase transition processes by the kinetics of small droplets formation (nucleation) dealt with in this work. Failure of simulated curves to agree with experimental data is the result of a situation in which droplets, when formed in the course of intercalation processes, show no tendency to merge and form large domains, later coalescing with the formation of a moving boundary between the diluted and concentrated coexisting phases. As follows from our previous work [16], nucleation and growth occurs during a short period of time when the concentration of inserted ions takes values between the binodal and spinodal points. Certainly, a phenomenological approach to nucleation and growth mechanism in lithiated graphite has revealed some similarities to classical electrocrystallization models, as in both cases, there is an increase in the total area of the interfaces between droplets of the new phase and the old phase [16]. A real challenge is to include nucleation and growth phenomena together with limiting interfacial ion-transfer kinetics into a phase-field model to describe coherently the concentration profile in intercalation electrodes during the entire time domain of phase transition.

Conclusion

In this paper, we try to understand the role of solid-state diffusion of ions during their insertion into host electrodes when this diffusion is coupled with some external kinetics, such as slow interfacial ion transfer (Butler–Volmer formulation), and formation of small droplets of new phase in the bulk of the old one because of the decrease in the free energy barrier between the two interfaces. For this purpose, we performed a numerical simulation of potential dependences of the differential intercalation capacitance, C_{dif}, the statistical factor of sites occupation, $X(1-X)$, and the chemical diffusion coefficient, D, for their further comparison with experimental data. It was shown that the shape of the potential dependences of D calculated according to a classical approach (Eq. 8a) is very convenient in distinguishing between the limitation of the intercalation reaction by one or the other alternative kinetics (interfacial, i.e., Butler–Volmer kinetics vs small droplets formation). Evaluation of errors in D, induced by incorrect application of essentially non-equilibrium values of differential intercalation capacitances, C_{dif}, in Eq. 8a has been done. The effect of the Butler–Volmer kinetics as the major, relevant RDS of the phase transition process and calculation of D was evaluated. We found that exact D values can be obtained up to compositions of the inserted ions, which relate to the binodal point. Beyond the binodal point, errors increase towards the spinodal point, which is in good agreement with the predictions of phase field models [17]. Within the spinodal domain, the potential dependence of D calculated by application of the Cottrellian model is entirely connected to the related potential dependence of C_{dif}. In this paper, we tried to rationalize an unusual, previously reported result: D vs X,E, which was calculated for the spinodal domain of LiC_{12} to LiC_6 phase transition, appeared to be approximately the same as that derived from the moving boundary model. It is believed that this result originates from a coupling of slow interfacial ion-transfer kinetics with a finite-space domain of the intercalation reaction. This coupling produces a sharp pseudo-Cottrellian peak from which the diffusion coefficient is calculated by a titration technique such as PITT. The formal diffusion coefficient reflects strong attractive interactions between the intercalation sites. According to the simple lattice gas approaches, segregation and phase separation during intercalation result from these strong interactions, which appear as sharp peaks of C_{dif} vs X,E in the phase transition domain. The formal calculation of D includes C_{dif}, and thereby D vs X,E calculated for electrodes, which undergo phase transition, exhibit always deep minima in the phase transition domains. The calculation of D in the spinodal domain (part of the entire phase transition domain) by a Cottrellian model will always give spurious values. We believe that the above described coupling between limitation by slow interfacial kinetics and the finite-space solid-state diffusion (part of the entire intercalation domain) explains the experimentally observed change in the character of the phase boundary movement from a linear to the square-root law.

Acknowledgement A partial support for our studies on transport phenomena during phase transitions is obtained by the GIF (German-Israel Foundation).

References

1. Wen CJ, Boukamp BA, Huggins RA, Weppner W (1979) J Electrochem Soc 126:2258
2. Weppner W, Huggins RA (1978) Ann Rev Mater Sci 8:269
3. Weppner W (1995) In: Bruce PG (ed) Solid-state electrochemistry, chapter 8. Cambridge University Press, Cambridge, UK, p 199
4. Ho C, Raistrick ID, Huggins RA (1980) J Electrochem Soc 127:343
5. Levi MD, Aurbach D (1999) Electrochimica Acta 45:167
6. Deiss E (2002) Electrochim Acta 47:4027
7. Eftekhari A (2005) Electrochim Acta 50:2541
8. Montella C (2006) Electrochim Acta 51:3102
9. Montella C (2002) J Electroanal Chem 518:61
10. Vorotyntsev MA, Levi MD, Aurbach D (2004) J Electroanal Chem 572:299
11. Levi MD, Demadrille R, Pron A, Vorotyntsev MA, Gofer Y, Aurbach D (2005) J Electrochem Soc 152:E61

12. Levi MD, Markevich E, Aurbach D (2005) J Phys Chem B 109:7420
13. Bard AJ, Faulkner LR (1980) Electroanalytical methods. Wiley, New York, p 92
14. Vorotyntsev MA, Badiali JP (1994) Electrochim Acta 39:289
15. McKinnon WR, Haering RR (1987) Modern aspects in electrochemistry, vol. 15. Plenum Press, New York, p 235
16. Levi MD, Markevich E, Aurbach D (2005) Electrochim Acta 51:98
17. Han BC, Van der Ven A, Morgan D, Ceder G (2004) Electrochim Acta 49:4691
18. Weppner W, Huggins RA (1977) J Electrochem Soc 124:1569
19. Levi MD, Aurbach D, Vorotyntsev MA (2002) Condensed Matter Physics 5:329
20. Naumana EB, He DQ (2001) Chem Eng Sci 56:1999
21. Levi MD, Aurbach D (1997) J Phys Chem B 101:4641
22. Levi MD, Wang C, Aurbach D, Chvoj Z (2004) J Electroanal Chem 562:187
23. Funabiki Atsushi, Inaba Minoru, Abe Takeshi, Ogumi Zempachi (1999) J Electrochem Soc 146:2443